Mechatronics and Intelligent Transportation Systems
https://www.acadlore.com/journals/MITS

Design and Testing of Cooperative Motion Controller for UAV-UGV System

Yuxue Li, Xiaoyuan Zhu*

School of Mechanical Engineering, Southeast University, 211189 Nanjing, China

* Correspondence: Xiaoyuan Zhu (zhuxy@seu.edu.cn)

Received: 08-12-2022 **Revised:** 09-10-2022 **Accepted:** 09-26-2022

Citation: Y. X. Li and X. Y. Zhu, "Design and testing of cooperative motion controller for UAV-UGV system," *Mechatron. Intell Transp. Syst.*, vol. 1, no. 1, pp. 12-23, 2022. https://doi.org/10.56578/mits010103.

© 2022 by the authors. Published by Acadlore Publishing Services Limited, Hong Kong. This article is available for free download and can be reused and cited, provided that the original published version is credited, under the CC BY 4.0 license.

Abstract: Unmanned ground vehicles (UGVs) and quadrotor unmanned aerial vehicles (UAVs) can work together to solve challenges like intelligent transportation, thanks to their excellent performance complements in perception, loading, and endurance. This study presents a UAV-UGV system cooperative control mechanism. To achieve collaborative trajectory tracking, the leader-follower strategy based on a centralized control structure is firstly established in conjunction with the application scenario. The fuzzy robust controller is created to control the quadrotor UAV and improve attitude stability. Meanwhile, the UGV's controller uses the pure pursuit algorithm and a proportional integral derivative (PID) controller. In order to evaluate the cooperative control strategy and algorithm, the UAV-UGV experimental platform is set up based on the QDrone and QCar, and the experimental results show the viability of the suggested plan.

Keywords: Unmanned ground vehicles (UGVs); Unmanned aerial vehicles (UAVs); Cooperative motion controller; Fuzzy robust controller

1. Introduction

Autonomous unmanned systems, such as unmanned aerial vehicles (UAVs) and unmanned ground vehicles (UGVs), have gradually gained public attention in recent years [1, 2]. Quadrotor UAVs can perform vertical take-off and landing, hovering, and complete flexible and agile movements. Their application potential is immense in aerial photography, intelligent distribution, and urban patrol, owing to their simple mechanical design and low cost [3]. The UAV's 3D motion characteristics result in a greater field of vision and perception, and fewer restrictions from obstacles [4].

Albeit the distinctive motion characteristics above, quadrotor UAVs nevertheless have several shortcomings when it comes to carrying out missions because of the limitations of the related technical development. Even though work on high-energy density batteries is currently progressing, UAVs fall short of UGV systems in terms of durability. The UGVs can operate nearly regardless of the endurance duration because they can be powered by engines and power batteries. However, in dense building clusters, UGVs' sensing range is limited, and communications are vulnerable to interference and disruptions [5]. The UAV-UGV synergistic systems can efficiently combine the advantages of the two and offer solutions that are not possible with only one unmanned system. Because of this, the UAV-UGV systems have a wide range of application requirements in both the military and civilian sectors, including environmental parameter monitoring in intelligent agriculture, assisted landing in complicated terrain, and post-disaster rescue [6].

Numerous studies have been done on the leader-follower strategy [7], the virtual structure method [8], the artificial potential field [9], and the behavior-based method [10] of UAV-UGV systems. A quadrotor UAV was utilized by Chamry et al. [11] to track the movements of a UGV and realize the takeoff or landing on the moving UGV platform. Askari et al. [12] used a virtual structure method along with formation input to build a centrally controlled quadrotor UAV formation flight. When there are several dynamic and static obstacles, Zhao et al. [13] developed an enhanced artificial potential field method coupled with formation division to provide more flexible formation avoidance of obstacles. Balch and Arkin [10] designed and applied new reactive behaviors to multi-robot formations, and combined formation behaviors with other navigation behaviors. In this way, the teams of

robots can avoid hazards, maintain formation, and reach navigation goals.

Due to its simple idea and minimal communication needs, the leader-follower system is easier to apply in engineering and is more frequently used in practice [14]. This research suggests a leader-follower cooperation technique for the UAV-UGV systems in conjunction with the application scenarios of intelligent transportation. The UGV is designated as the leader of the collaborative system to conduct course planning based on environmental maps, for UGVs are more susceptible to traffic limitations. The follower UAV's motion planning is accomplished through the cooperative controller, combined with the states of the UGV. Pure pursuit is used to achieve the motion control of the UGV in the low-velocity situation. The quadrotor UAV uses a dual-loop control structure, with the position subsystem in the outer loop and the attitude subsystem in the inner loop. When the attitude is controlled, the motion robustness and attitude stability are improved thanks to the fuzzy robust controller. The UAV-UGV experimental platform is constructed using Quanser QCar and QDrone, and trajectory tracking tests are run to assess the efficiency of the cooperative control strategy and algorithm.

The remainder of this paper is divided into five sections: Section 2 establishes mathematical models of the UAV-UGV cooperative system; Section 3 proposes the collaborative control strategy based on the leader-follower method, and designs the controller; Section 4 introduces the experimental platform and verifies the proposed strategy; Section 5 draws the main conclusions.

2. Problem Statement

2.1 UGV Motion Model

In the inertial coordinate system, the states of the UGV are described by $P_c = [x_r, y_r, \psi_c]^T$, where x_r and y_r represent the position coordinates at the midpoint of the rear axis, respectively, and ψ_c represents the vehicle orientation whose positive direction is taken counterclockwise from the X-axis. Suppose the wheels purely roll during low-velocity driving, and the UGV travels at the velocity of *V*. In Figure 1, *E* represents the axis of the real axis with coordinates $[x_r, y_r]$, *F* represents the axis of the front with coordinates $[x_f, y_f]$, *C* represents the intersection of the front wheel *FC* and the rear wheel normal *EC*, *R* represents the steering radius, δ represents the turning angle of the front wheel, and *l* represents the wheelbase of the UGV.

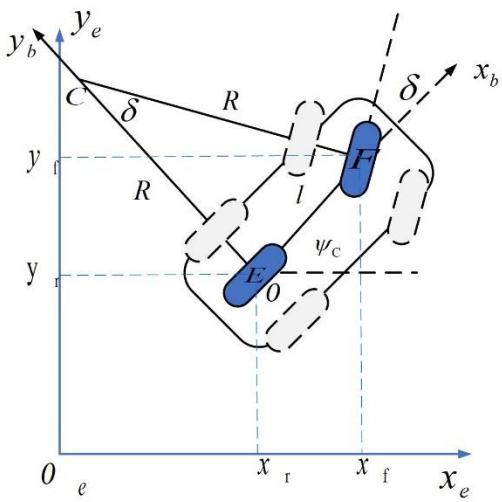

Figure 1. The UGV motion model

Then, the kinematic model of the UGV can be established as [15]:

$$\begin{cases} \dot{x}_r = V\cos\psi_c \\ \dot{y}_r = V\sin\psi_c \\ \dot{\psi}_c = V\tan\delta / l \end{cases} \tag{1}$$

2.2 Quadrotor UAV Dynamic Model

As shown in Figure 2, the position and attitude of the quadrotor UAV can be described using two coordinate systems, namely, the inertial coordinate system $O_eX_eY_eZ_e$ and the body coordinate system $O_bX_bY_bZ_b$. In this

paper, our coordinate system is oriented in the counterclockwise direction, and the orientation is determined by the right-hand rule. $\boldsymbol{X}=[x,y,z]^T$ and $\boldsymbol{V}=[u,v,w]^T$ denote the center of the mass position and linear velocity in the inertial coordinate system, respectively; $[\phi,\theta,\psi]^T$ denote the UAV attitude angle; $[p,q,r]^T$ denote the roll, pitch, and yaw angular velocities of rotation around the body axis, respectively.

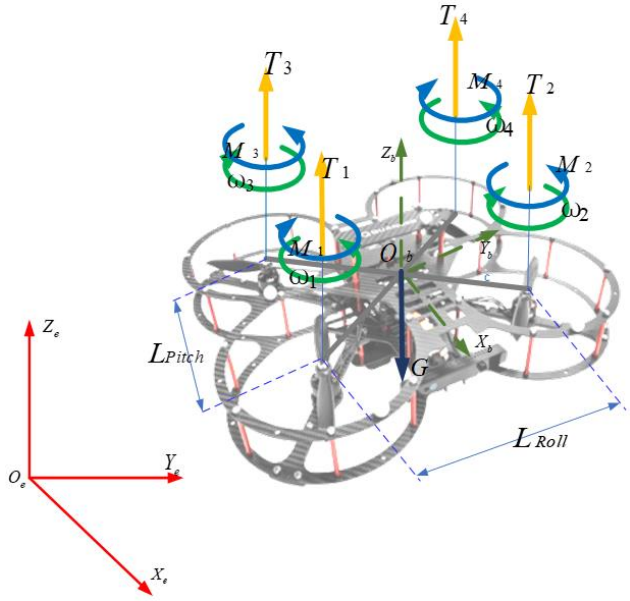

Figure 2. Force analysis of the quadrotor UAV

According to the Newton-Euler formula, the UAV's motion can be modeled as [4]:

$$\begin{aligned} m\dot{\boldsymbol{V}} &= -\boldsymbol{G}^{e} + \boldsymbol{T}^{\boldsymbol{b}}\boldsymbol{R}_{\boldsymbol{b}}^{\boldsymbol{e}} \\ \boldsymbol{M} &= \boldsymbol{J}\dot{\boldsymbol{\omega}} + \boldsymbol{\omega}\times\boldsymbol{J}\boldsymbol{\omega} \end{aligned} \tag{2}$$

where, R_b^e is the rotation matrix from the body coordinate system to the inertial coordinate system in the order of ψ-θ-ϕ; J is the inertial matrix of the quadrotor UAV; M is the combined moment, including rotor lift moment, anti-torsional pitch, and gyroscopic moment.

Considering the structural symmetry, the moment of inertia generated by the rotation of the rotor can be described as a diagonal matrix $J_{RP}=diag(J_{rx}, J_{ry}, J_{rz})$. Substituting the matrix into the above equation, the nonlinear dynamics of the quadrotor UAV can be obtained as [4]:

$$\begin{aligned} \ddot{x} &= \frac{T}{m}(\cos\phi\sin\theta\cos\psi + \sin\phi\sin\psi) \\ \ddot{y} &= \frac{T}{m}(\cos\phi\sin\theta\sin\psi - \sin\phi\cos\psi) \\ \ddot{z} &= \frac{T}{m}\cos\phi\cos\theta \\ \ddot{\phi} &= \frac{J_y - J_z}{J_x}\dot{\theta}\dot{\psi} + \frac{J_{rz}}{J_x}(-\omega_1+\omega_2-\omega_3+\omega_4)\dot{\theta} + \frac{\Gamma\phi}{J_x} \\ \ddot{\theta} &= \frac{J_z - J_x}{J_y}\dot{\phi}\dot{\psi} - \frac{J_{rz}}{J_y}(-\omega_1+\omega_2-\omega_3+\omega_4)\dot{\phi} + \frac{\Gamma\theta}{J_y} \\ \ddot{\psi} &= \frac{J_x - J_y}{J_z}\dot{\phi}\dot{\theta} + \frac{\Gamma\psi}{J_z} \end{aligned} \tag{3}$$

2.3 UAV-UGV Cooperative Model

In a cooperative system, the motion states of the adjacent unmanned vehicles need to be considered in path

planning. As shown in Figure 3, the individual unmanned vehicles (UVs) within the cooperative system can be illustrated by a point set $V(G)=\{V_1,V_2\}$, and the information exchange between the UVs by an edge set $E(G)=\{(V_1,V_2),(V_2,V_1)\}$. Note that (V_i,V_j) indicates that information can be transmitted from V_i to V_j.

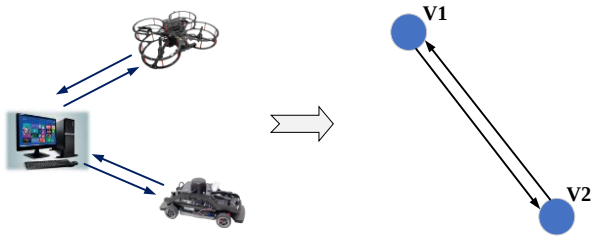

Figure 3. UAV-UGV cooperative system

The interaction intensity between UVs can be described by an adjacency matrix $W=[w_{ij}]$. In the directed graph, if there are edges pointing from V_i to V_j, then w_{ij} is equal to the weight of the influence. If $i=j$ and $w_{ij}=0$, and if no edges point from V_i to V_j, then $w_{ij}=\infty$.

The degree matrix of the directed graph is denoted as $D=\mathrm{diag}\{d_1,d_2,\ldots,d_n\}$, where $d_i=\sum_{j=1}^{n} w_{ij}$. The Laplacian matrix of the directed graph is $L=D-W$. Ignoring the system difference in motion features, UVs can be regarded as abstract points in the collaborative system.

As shown in Figure 3, the adjacency of the UAV-UGV system is $W_{1,2}=\begin{pmatrix}0 & 1\\ 1 & 0\end{pmatrix}$. It is generally considered that the UGV travels on a plane, and its motion state can be represented by $\boldsymbol{x}_G=[x_{UGV},y_{UGV},\psi_{UGV}]^T$. Meanwhile, the quadrotor UAV moves in the three-dimensional space with motion states $\boldsymbol{x}_A=[x_{UAV},y_{UAV},z_{UAV},\phi_{UAV},\theta_{UAV},\psi_{UAV}]^T$. The number of the state variables should be unified to facilitate subsequent information processing and enhance the feasibility of the collaborative system.

Position control is getting more attention from researchers of the cooperative system. The height control and planar motion control can be decoupled, so that the cooperative system only needs to consider the motion of the UAV in the X and Y directions. Thus, the UAV states can be expressed as $x_A=[x_{UAV},y_{UAV},z_{UAV}]^T$. In summary, the UAV-UGV cooperative system can be modeled as:

$$\begin{aligned}\dot{\boldsymbol{x}}_A &= \boldsymbol{v}_A\\ \dot{\boldsymbol{v}}_A &= \boldsymbol{u}_A\\ \dot{\boldsymbol{x}}_G &= \boldsymbol{u}_G\end{aligned} \tag{4}$$

3. Design of Cooperative Controller

In the general urban scene (Figure 4), the UGV encounters a more complicated traffic environment, a variety of impediments, and numerous unanticipated hazards, all of which necessitate better real-time decision-planning. In addition, the UGV functions more as an executor in a system due to its huge loading capacity. By contrast, the quadrotor UAVs' path planning involves less consideration of external obstacles, and they are known for their quick maneuvering. These UAVs serve more as the system's "eye" and perform perceptual tasks.

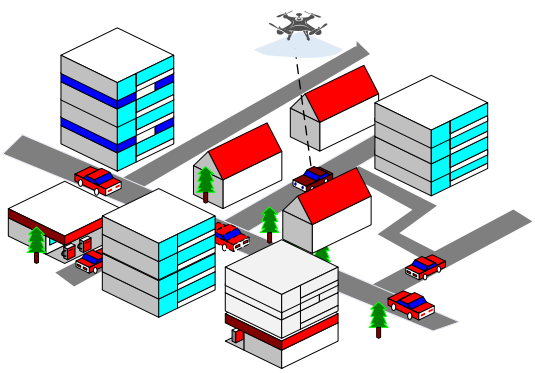

Figure 4. Application scenario

As a result, this study chooses a leader-follower method-based collaborative approach. While the UAV follows the movement of the UGV and provides environmental information, the UGV is the leader and plans the path in accordance with the traffic environment it must navigate. The UAV's sensing data can improve the predictability and dependability of decision-making. The leader-follower strategy is simpler to apply in engineering applications and requires less communication skill.

The UAV must fly around the UGV for its role in the system is to sense environmental data about the immediate area surrounding the UGV. The relative distance between the UAV and the UGV must satisfy the formation requirement during motion, so that the UAV can be brought into the desired position:

$$\begin{cases} \mathbf{x}_{RF}(t) = \mathbf{x}_L(t) + \dfrac{L(t)(\mathbf{x}_F(t) - \mathbf{x}_L(t))}{\|\mathbf{x}_F(t) - \mathbf{x}_L(t)\|} \\ \psi_{RF}(t) = \psi_L(t) \end{cases} \tag{5}$$

where, $x_{RF} = [x_{RF}, y_{RF}]^T$ and ψ_{RF} are the reference trajectory of the follower; $\boldsymbol{x}_L = [x_{UGV}, y_{UGV}]^T$; $\boldsymbol{x}_F = [x_{UAV}, y_{UAV}]^T$; $\psi_L = \psi_{UGV}$.

3.1 Fuzzy Robust Controller of UAV

With the position subsystem acting as the outer loop and the attitude subsystem acting as the inner loop, the quadrotor UAV adopts a dual-loop structure. After a rough linearization close to the equilibrium point, the proportional-integral-derivative (PID) controller is used for the quadrotor UAV's position subsystem [16]. Given the inevitable disturbances during flight, such as wind perturbations, the attitude subsystem of the UAV is developed using a fuzzy robust controller to increase attitude stability and anti-disturbance capacity. Prior to building the attitude controller, the attitude subsystem must first be linearized. A nonlinear system is fitted to a collection of linear systems using the T-S fuzzy model, whose fundamental premise is to linearize at numerous operational points [17]. The UAV is supposed to conduct a modest angle maneuver, without considering the impact of gyroscopic moment. Thus, the attitude subsystem can be modeled by:

$$\begin{aligned} \ddot{\phi} &= \frac{J_y - J_z}{J_x}\dot{\theta}\dot{\psi} + \frac{\Gamma_\phi}{J_x} \\ \ddot{\theta} &= \frac{J_z - J_x}{J_y}\dot{\phi}\dot{\psi} + \frac{\Gamma_\theta}{J_y} \\ \ddot{\psi} &= \frac{J_x - J_y}{J_z}\dot{\phi}\dot{\theta} + \frac{\Gamma_\psi}{J_z} \end{aligned} \tag{6}$$

Setting the state vector as $\boldsymbol{x} = [\phi \quad \theta \quad \psi \quad \dot{\phi} \quad \dot{\theta} \quad \dot{\psi}]^T$, the state space of the attitude subsystem can be expressed as:

$$\dot{\boldsymbol{x}} = \boldsymbol{A}(\boldsymbol{x})\boldsymbol{x}(t) + \boldsymbol{B}(\boldsymbol{x})\boldsymbol{u}(t) \tag{7}$$

where,

$$\boldsymbol{u} = \begin{bmatrix} \Gamma_\phi & \Gamma_\theta & \Gamma_\psi \end{bmatrix}^T$$

$$\mathbf{y} = \begin{bmatrix} \phi & \theta & \psi & \dot{\phi} & \dot{\theta} & \dot{\psi} \end{bmatrix}^T$$

$$\boldsymbol{A}(\boldsymbol{x}) = \begin{bmatrix} 0 & 0 & 0 & 1 & 0 & 0 \\ 0 & 0 & 0 & 0 & 1 & 0 \\ 0 & 0 & 0 & 0 & 0 & 1 \\ 0 & 0 & 0 & 0 & 0 & \dfrac{J_y - J_z}{J_x}\dot{\theta} \\ 0 & 0 & 0 & 0 & 0 & \dfrac{J_z - J_x}{J_y}\dot{\phi} \\ 0 & 0 & 0 & \dfrac{J_x - J_y}{J_z}\dot{\theta} & 0 & 0 \end{bmatrix}$$

$$\boldsymbol{B}(\boldsymbol{x})=\begin{bmatrix}0 & 0 & 0 & 1/J_x & 0 & 0\\ 0 & 0 & 0 & 0 & 1/J_y & 0\\ 0 & 0 & 0 & 0 & 0 & 1/J_z\end{bmatrix}^T$$

The fuzzy premise variables can be selected as [17]:

$$\mu_1(t)=\dot{\phi}\quad \mu_2(t)=\dot{\theta}\quad \mu_3(t)=\dot{\psi} \tag{8}$$

Suppose the angular velocity is within a certain range:

$$\mu_{iMin}<\mu_i<\mu_{iMax}, i=1,2,3 \tag{9}$$

The number of weight functions is p=3. Thus, the number of fuzzy rules for the UAV system is $r=2^3=8$. The if-then rules for the fuzzy model can be expressed as:

$$\begin{gathered}IF\left(\mu_1=\mu_{1Max},\mu_2=\mu_{2Max},\mu_3=\mu_{3Max}\right),THENSubsystem_1\\ \vdots\\ IF\left(\mu_1=\mu_{1Min},\mu_2=\mu_{2Min},\mu_3=\mu_{3Min}\right),THENSubsystem_8\end{gathered} \tag{10}$$

$$Subsystem_i=\begin{cases}\dot{\boldsymbol{x}}=\boldsymbol{A}_i\boldsymbol{x}(t)+\boldsymbol{B}_i\boldsymbol{u}(t)\\ \boldsymbol{y}(t)=\boldsymbol{C}_i\boldsymbol{x}(t)\end{cases} i=1,2,...,8 \tag{11}$$

The T-S fuzzy model of the attitude subsystem can be expressed as

$$\begin{aligned}\dot{\boldsymbol{x}}&=\textstyle\sum_{i=1}^{8}h_i(\mu_i)\{\boldsymbol{A}_i\boldsymbol{x}(t)+\boldsymbol{B}_i\boldsymbol{u}(t)\}\\ \boldsymbol{y}(t)&=\boldsymbol{C}_i\boldsymbol{x}(t)\end{aligned} \tag{12}$$

where, h_i is the membership functions:

$$\begin{aligned}&h_1(\mu_i)=M_1^1*M_2^1*M_3^1 \quad h_2(\mu_i)=M_1^2*M_2^1*M_3^1\\ &h_3(\mu_i)=M_1^1*M_2^2*M_3^1 \quad h_4(\mu_i)=M_1^2*M_2^2*M_3^1\\ &h_5(\mu_i)=M_1^1*M_2^1*M_3^2 \quad h_6(\mu_i)=M_1^2*M_2^1*M_3^2\\ &h_7(\mu_i)=M_1^1*M_2^2*M_3^2 \quad h_8(\mu_i)=M_1^2*M_2^2*M_3^2\end{aligned}$$

The weighting functions M_i^j can be expressed as:

$$\begin{gathered}M_i^1=\frac{\mu_{iMax}-\mu_i(t)}{\mu_{iMax}-\mu_{iMin}}\\ M_i^2=\frac{\mu_i(t)-\mu_{iMin}}{\mu_{iMax}-\mu_{iMin}}\\ i=1,2,3\end{gathered}$$

$$A_i=\begin{bmatrix}A_{i1} & A_{i2}\\ A_{i3} & A_{i4}\end{bmatrix}, A_{i4}=\begin{bmatrix}0 & 0 & \frac{J_y-J_z}{J_x}\mu_{2i}\\ 0 & 0 & \frac{J_z-J_x}{J_y}\mu_{1i}\\ \frac{J_x-J_y}{J_z}\mu_{1i} & 0 & 0\end{bmatrix}$$

$$\mu_{1i} = [\mu_{1Min} \quad \mu_{1Max} \quad \mu_{1Min} \quad \mu_{1Max} \quad \mu_{1Min} \quad \mu_{1Max} \quad \mu_{1Min} \quad \mu_{1Max}]$$
$$\mu_{2i} = [\mu_{2Min} \quad \mu_{2Min} \quad \mu_{2Max} \quad \mu_{2Max} \quad \mu_{2Min} \quad \mu_{2Min} \quad \mu_{2Max} \quad \mu_{2Max}]$$
$$\mu_{3i} = [\mu_{3Min} \quad \mu_{3Min} \quad \mu_{3Min} \quad \mu_{3Min} \quad \mu_{3Max} \quad \mu_{3Max} \quad \mu_{3Max} \quad \mu_{3Max}]$$

Based on the T-S fuzzy model, the controller designed for the attitude subsystem can be expressed as:

$$u = \sum_{j=1}^{8} h_j(\mu_i)\{K_{fuzzy}x\} \tag{13}$$

$$\dot{\boldsymbol{x}} = \sum_{i=1}^{8}\sum_{j=1}^{8} h_i h_j \{\boldsymbol{A}_i + \boldsymbol{B}_i \boldsymbol{K}_j\}\boldsymbol{x}(t) \tag{14}$$

The fuzzy state control law should satisfy $\lim_{t\to\infty} x(t) = 0$. Moreover, the pole distribution of the closed-loop fuzzy control system is limited to a predetermined region D, such that the system can make transient responses:

$$\sigma(\boldsymbol{A_i} + \boldsymbol{B_i}\boldsymbol{K_j}) \subset \boldsymbol{D} \tag{15}$$

Theorem 1 [18]: The closed-loop system (14) can achieve asymptotic stabilization, if and only if there exists a common positive symmetric matrix $\boldsymbol{P}$ such that:

$$\begin{aligned} &(\boldsymbol{A}_i + \boldsymbol{B}_i\boldsymbol{K}_i)\boldsymbol{P}^T + \boldsymbol{P}(\boldsymbol{A}_i + \boldsymbol{B}_i\boldsymbol{K}_i) < 0, i = 1,2,...,8 \\ &\boldsymbol{G}_{ij}\boldsymbol{P}^T + \boldsymbol{P}\boldsymbol{G}_{ij} < 0, i < j < 8 \\ &\boldsymbol{G}_{ij} = \boldsymbol{A}_i + \boldsymbol{B}_i\boldsymbol{K}_j + \boldsymbol{A}_j + \boldsymbol{B}_j\boldsymbol{K}_i \end{aligned} \tag{16}$$

$\boldsymbol{Q_s} = \boldsymbol{P}^{-1}, \boldsymbol{Y_i} = \boldsymbol{K_i}\boldsymbol{Q_s}$. The quadratic stability problem of the system can be converted into the feasibility problem of linear matrix inequality.

Theorem 2 [18]: The closed-loop system (14) is stable if there exists a common positive symmetric matrix Q_s and matrix Y_{si} such that the following LMI condition holds:

$$\begin{aligned} &\boldsymbol{A_i}\boldsymbol{Q}_S + \boldsymbol{Q_S}\boldsymbol{A_i^T} + \boldsymbol{B_i}\boldsymbol{Y_{si}} + \boldsymbol{Y_{si}^T}\boldsymbol{B}_i^T < 0, i = 1,2,...,8 \\ &\boldsymbol{A}_i\boldsymbol{Q}_S + \boldsymbol{Q}_S\boldsymbol{A}_i^T + \boldsymbol{B}_i\boldsymbol{Y}_{Sj} + \boldsymbol{Y}_{Sj}^T\boldsymbol{B}_i^T + \boldsymbol{A}_j\boldsymbol{Q}_S + \boldsymbol{Q}_S\boldsymbol{A}_j^T + \boldsymbol{B}_j\boldsymbol{Y}_{Si} + \boldsymbol{Y}_{Si}^T\boldsymbol{B}_j^T < 0, i < j \le 8 \end{aligned} \tag{17}$$

The fuzzy state feedback gain is $\boldsymbol{K}_{si} = \boldsymbol{Y}_{si}\boldsymbol{Q}_s^{-1}$. It is assumed that the pole configuration area D is a circular area with the center of $(-q, 0)$ and the radius of r:

$$D = \left\{ s \in C : \boldsymbol{L} + s\boldsymbol{M} + \bar{s}\boldsymbol{M}^T < 0 \right\} \tag{18}$$

where, $\boldsymbol{L} = \begin{bmatrix} r & q \\ q & -r \end{bmatrix}, \boldsymbol{M} = \begin{bmatrix} 0 & 1 \\ 0 & 0 \end{bmatrix}$.

Theorem 3 [19]: The closed-loop fuzzy system (14) is D-stable if there exists a common positive symmetric matrix Q_p and matrix Y_{pi} such that the following LMI condition holds:

$$\begin{bmatrix} -r\boldsymbol{Q}_p & q\boldsymbol{Q}_p + \boldsymbol{Q}_p\boldsymbol{A}_i^T + \boldsymbol{Y}_{pi}^T\boldsymbol{B}_i^T \\ q\boldsymbol{Q}_p + \boldsymbol{A_i}\boldsymbol{Q}_p + \boldsymbol{B_i}\boldsymbol{Y_{pi}} & -r\boldsymbol{Q_p} \end{bmatrix} < 0, i = 1,2,...,8 \tag{19}$$

The state feedback gain is $K_{pi} = Y_{pi}Q_p^{-1}$.

Theorem 4 [17, 19]: The closed-loop fuzzy system (14) is stable in the specified region D if there exists a common positive symmetric matrix Q and matrix Y_i such that the following LMI condition holds:

$$\begin{aligned}
&\boldsymbol{A_iQ}+\boldsymbol{QA_i^T}+\boldsymbol{B_iY_i}+\boldsymbol{Y_i^TB_i^T}<0, i=1,2,...,8\\
&\boldsymbol{A_iQ}+\boldsymbol{QA_i^T}+\boldsymbol{B_iY_j}+\boldsymbol{Y_j^TB_i^T}+\boldsymbol{A_jQ}+\boldsymbol{QA_j^T}+\boldsymbol{B_jY_i}+\boldsymbol{Y_i^TB_j^T}<0, i<j\le 8\\
&\begin{bmatrix} -r\boldsymbol{Q} & q\boldsymbol{Q}+\boldsymbol{QA_i^T}+\boldsymbol{Y_i^TB_i^T}\\ q\boldsymbol{Q}+\boldsymbol{A_iQ}+\boldsymbol{B_iY_i} & -r\boldsymbol{Q}\end{bmatrix}<0, i=1,2,...,8
\end{aligned} \tag{20}$$

The fuzzy robust control gain is $K_i = Y_iQ^{-1}, i = 1,2,\ldots,8$.

3.2 Design of UGV Controller

The lateral control is realized by the pure pursuit algorithm. In Figure 5, the target point (x_g, y_g) that needs to be reached at the next moment is determined according to the preview distance. Based on the geometric relationship, we have:

$$\begin{aligned}
&\alpha = \tan^{-1}\frac{y_g}{x_g}\\
&\frac{L_d}{\sin(2\alpha)} = \frac{R}{\sin(\frac{\pi}{2}-\alpha)}
\end{aligned} \tag{21}$$

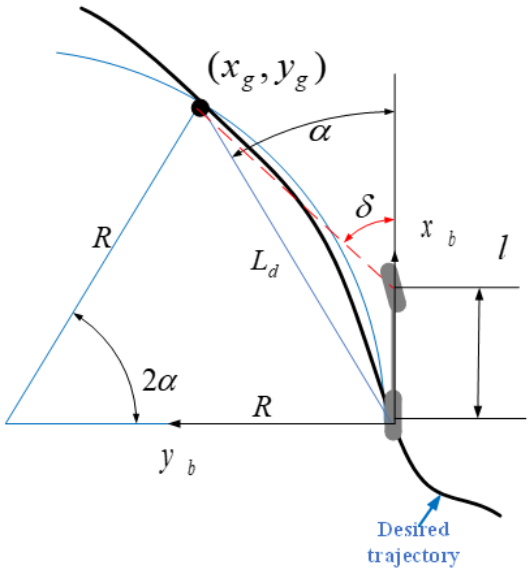

Figure 5. Pure pursuit method

The desired rotation angle of the front wheel can be derived by:

$$\delta = \tan^{-1}\frac{2l\sin\alpha}{L_d} \tag{22}$$

The proportional-integral (PI) and feedforward controllers are adopted to control longitudinal velocity. The velocity control input can be expressed as:

$$\begin{aligned}
&U_G = K_f V_d + K_p e_v + K_i \int e_v dt\\
&e_v = V_d - V
\end{aligned} \tag{23}$$

4. Experimental Testing

Figure 6 depicts the experimental platform of the UAV-UGV system, which consists of the QCar intelligent vehicle, QDrone quadrotor, Optitrack motion capture system, and ground workstation PC. The 10 cameras of the Optitrack motion capture system send the workstation the acquired position data over data lines. The workstation combines and processes the acquired data to determine the location and attitude information of UAV and UGV. Then, it generates the appropriate cooperative control command in accordance with the cooperative motion requirements. The information and control command between them are transmitted through a 5GHz WiFi network.

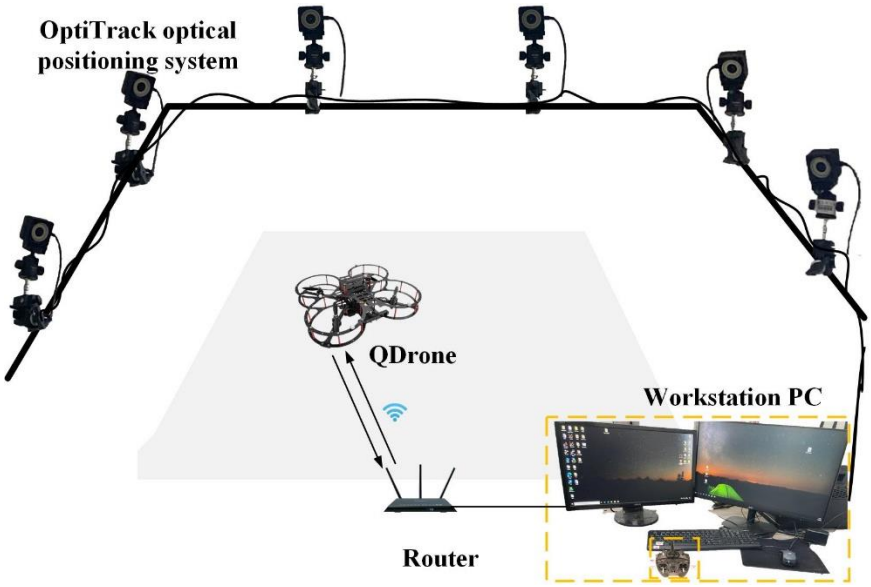

Figure 6. Experimental platform of the UAV-UGV system

The UGV's initial position in the defined coordinate system is (-2,-0.2), and its final position is (0.5,1.6). The Matlab/Simulink program simultaneously executes the quadrotor UAV procedure, the UGV control method, and the mission server procedure. As depicted in Figure 7, when the take-off command is sent, the UAV, which was initially parked close to the UGV, takes off and hovers above the initial position. The cooperative motion mode is then activated. The UAV-UGV system monitors the movement of the desired trajectory.

Figure 7. UAV-UGV cooperative trajectory experiment

The UGV tracks the planned path, and the quadrotor UAV follows the motion of the UGV at a height of 1m. The forward-looking direction of the UAV during the movement is consistent with the velocity direction of the UGV, such as to provide a better view field and capture the information about the UGV surroundings. The whole collaborative motion progress and the actual spatial trajectory are displayed in Figure 8.

The trajectory curve of the UGV (Figure 9) reveals that the longitudinal and lateral errors are less than 0.1m. Figure 10 and Figure 11 demonstrate the quadrotor UAV performance in cooperative motion. The actual flight trajectory is shown as the solid blue line in Figure 10, while the X and Y reference trajectories are shown as the

red dashed lines, which were generated online based on the real-time position state of the UGV and the formation requirements. The motion in Z-axis is set to a fixed height of 1m. The reference yaw angle in Figure 11 was also generated online based on the real-time forward direction of the UGV, which is equal to the UGV's direction angle. The tracking errors in the X and Y directions are smaller than 0.08m and 0.09m, respectively, and the tracking error of the yaw angle is below 10 degrees.

The above results demonstrated that the UAV is capable of stable flight in close proximity to the UGV, which preserves the consistency of direction and position to deliver ongoing information on the UGV's surroundings. To produce stable aerial images, the UAV's attitude must be maintained stably during the movement. The quadrotor UAV's error in height direction is 0-0.1m, while the absolute values of pitch and roll angles may vary by 0 to 5 degrees. The in-flight attitudes are stable and satisfy the requirements of the cooperative motion scenario.

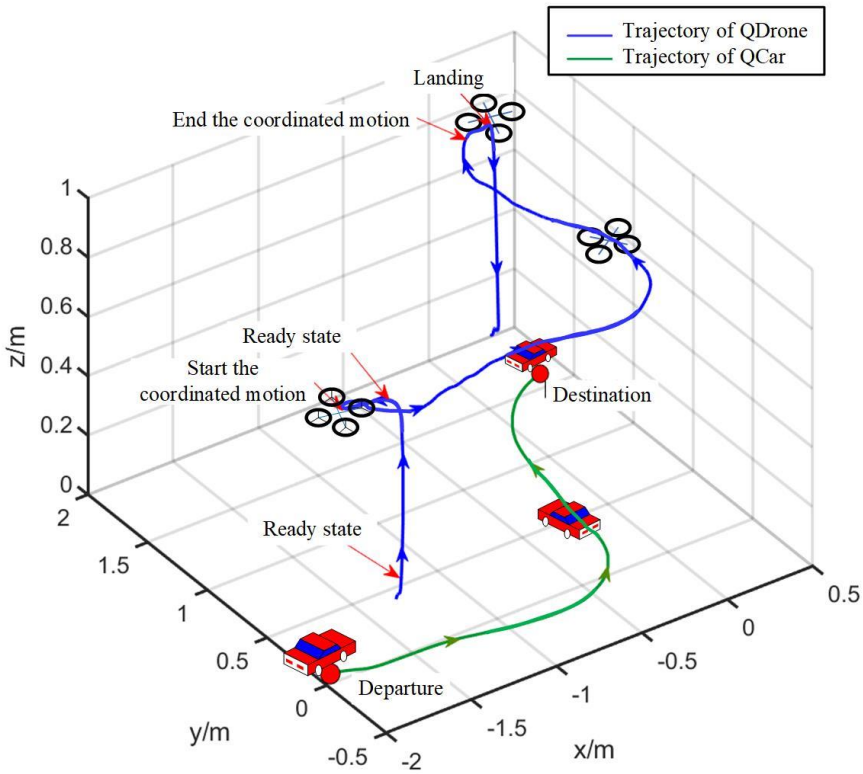

Figure 8. Trajectory of the UAV-UGV cooperative system

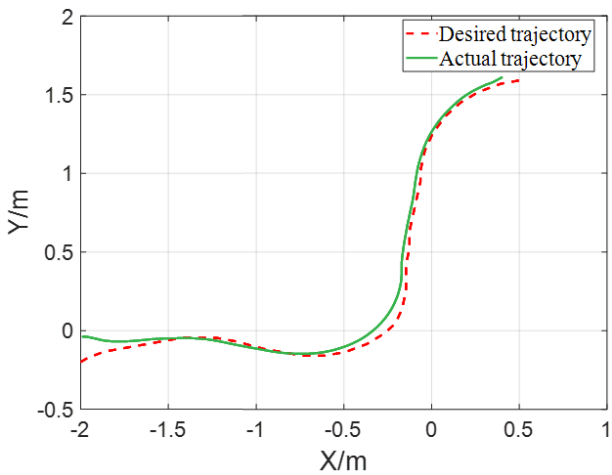

Figure 9. Trajectory of the UGV

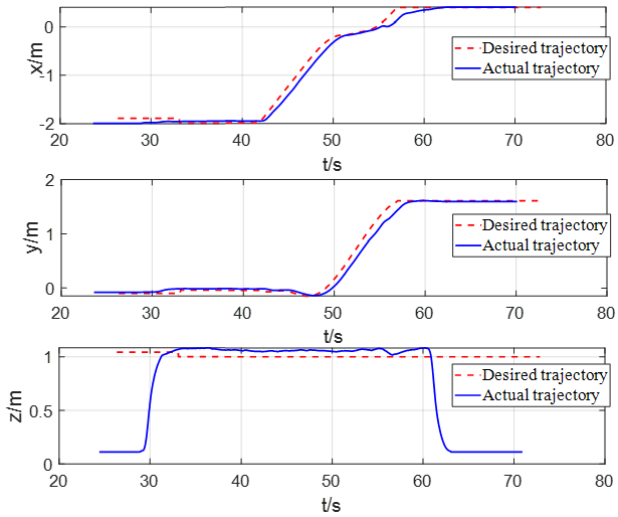

Figure 10. Trajectory of the UAV

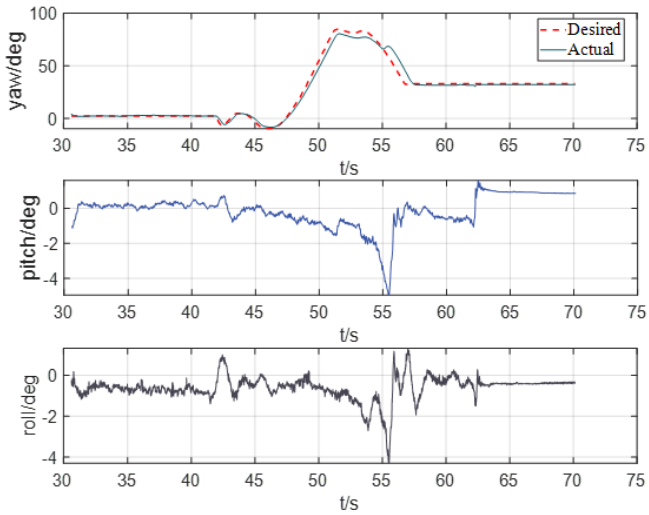

Figure 11. Attitude of the UAV

5. Conclusions

This study developed and tested a cooperative strategy for the UAV-UGV system based on the leader-follower method. First of all, the UAV-UGV system's leader-follower strategy was suggested while taking into account the urban traffic environment. The UGV took charge of the collaborative system since it was subject to stricter traffic limitations. As the follower, the UAV was in charge of various environmental perceptions. The UGV's states and cooperative motion requirements were used to create the UAV's position commands. Second, the UGV's horizontal and longitudinal motion control were implemented using the pure pursuit method and the proportional-integral controller, respectively. The dual-loop control mechanism was adopted by the quadrotor UAV. The position subsystem utilizes the PID contorller. To improve attitude stability and motion robustness, the attitude subsystem was linearized utilizing a T-S fuzzy model and a fuzzy robust controller. Finally, the experimental platform for the QCar and QDrone-based cooperative system was constructed to run tests for trajectory tracking. The reliability and efficiency of the cooperative control strategy and control algorithm were confirmed by the experimental results.

Data Availability

The data used to support the findings of this study are available from the corresponding author upon request.

Conflicts of Interest

The authors declare that they have no conflicts of interest.

Reference

[1] J. Li, G. Deng, C. Luo, Q. Lin, Q. Yan, and Z. Ming, "A hybrid path planning method in unmanned air/ground vehicle (UAV/UGV) cooperative systems," *IEEE T. Veh. Technol.*, vol. 65, no. 12, pp. 9585-9596, 2016. https://doi.org/10.1109/TVT.2016.2623666.

[2] J. Chen, X. Zhang, B. Xin, and H. Fang, "Coordination between unmanned aerial and ground vehicles: A taxonomy and optimization perspective," *IEEE Trans. Cybern.*, vol. 46, no. 4, pp. 959-972, 2016. https://doi.org/10.1109/TCYB.2015.2418337.

[3] J. Ghommam and M. Saad, "Autonomous landing of a quadrotor on a moving platform," *IEEE Trans. Aerosp. Electron. Syst.*, vol. 53, no. 3, pp. 1504-1519, 2017. https://doi.org/10.1109/TAES.2017.2671698.

[4] D. J. Almakhles, "Robust backstepping sliding mode control for a quadrotor trajectory tracking application," *IEEE Access*, vol. 8, pp. 5515-5525, 2020. https://doi.org/10.1109/ACCESS.2019.2962722.

[5] K. Nikolakopoulos, P. Lampropoulou, E. Fakiris, D. Sardelianos, and G. Papatheodorou, "Synergistic use of UAV and USV data and petrographic analyses for the investigation of beachrock formations: A case study from Syros Island, Aegean Sea, Greece," *Mineral-Basel*, vol. 8, no. 11, pp. 534-534, 2018. https://doi.org/10.3390/min8110534.

[6] S. Çaşka and A. Gayretli, "A survey of UAV/UGV collaborative systems," *CIE44&IMSS*, vol. 14, pp. 453-463, 2014.

[7] M. A. Dehghani, M. B. Menhaj, and M. Azimi, "Leader-follower formation control using an onboard leader tracker," In 2016 4th International Conference on Control, Instrumentation, and Automation, (ICCIA), Qazvin, Iran, 27-28 January 2016, pp. 99-104. https://doi.org/10.1109/ICCIAutom.2016.7483143.

[8] R. W. Beard, J. Lawton, and F. Y. Hadaegh, "A coordination architecture for spacecraft formation control," *IEEE Trans. Contr. Syst. Technol.*, vol. 9, no. 6, pp. 777-790, 2001. https://doi.org/10.1109/87.960341.

[9] Z. L. Nie, X. J. Zhang, and X. M. Guan, "UAV formation flight based on artificial potential force in 3D environment," In 2017 29th Chinese Control and Decision Conference, (CCDC), Chongqing, China, 17 July 2017, IEEE, pp. 5465-5470. https://doi.org/10.1109/CCDC.2017.7979468.

[10] T. Balch and R. C. Arkin, "Behavior-based formation control for multirobot teams," *IEEE Trans. Robot. Automat.*, vol. 14, no. 6, pp. 926-939, 1998. https://doi.org/10.1109/70.736776.

[11] K. A. Ghamry, Y. Dong, M. A. Kamel, and Y. Zhang, "Real-time autonomous take-off, tracking and landing of UAV on a moving UGV platform," In 2016 24th Mediterranean Conference on Control and Automation, (MED), Athens, Greece, June 21-24, 2016, IEEE, pp. 1236-1241. https://doi.org/10.1109/MED.2016.7535886.

[12] A. Askari, M. Mortazavi, and H. A. Talebi, "UAV formation control via the virtual structure approach," *J. Aerosp. Eng.*, vol. 28, no. 1, Article ID: 04014047, 2015. https://doi.org/10.1061/(ASCE)AS.1943-5525.0000351.

[13] Y. Zhao, L. Jiao, R. Zhou, and J. Zhang, "UAV formation control with obstacle avoidance using improved artificial potential fields," In 2017 36th Chinese Control Conference, (CCC), Dalian, China, July 26-28, 2017, IEEE, pp. 6219-6224. https://doi.org/10.23919/ChiCC.2017.8028347.

[14] A. S. Brandao, M. Sarcinelli-Filho, and R. Carelli, "Leader-follower control of a UAV-UGV formation," In 2013 16th International Conference on Advanced Robotics, (ICAR), Montevideo, Uruguay, November 25-29, 2013, IEEE, pp. 1-6. https://doi.org/10.1109/ICAR.2013.6766592.

[15] J. Hu, Y. Zhang, and S. Rakheja, "Adaptive trajectory tracking for car-like vehicles with input constraints," *IEEE Trans. Ind. Electron.*, vol. 69, no. 3, pp. 2801-2810, 2022. https://doi.org/10.1109/TIE.2021.3068672.

[16] C. Liu, J. Pan, and Y. Chang, "PID and LQR trajectory tracking control for an unmanned quadrotor helicopter: Experimental studies," In 2016 35th Chinese Control Conference, (CCC), Chengdu, China, August 29, 2016, IEEE, pp. 10845-10850. https://doi.org/10.1109/ChiCC.2016.7555074.

[17] H. Lee and H. J. Kim, "Robust control of a quadrotor using Takagi-Sugeno fuzzy model and an LMI approach," In 2014 14th International Conference on Control, Automation and Systems, (ICCAS 2014), Gyeonggi do, Korea, October 22-25, 2014, IEEE, pp. 370-374. https://doi.org/10.1109/ICCAS.2014.6988024.

[18] F. Torres, A. Rabhi, D. Lara, G. Romero, and C. Pégard, "Fuzzy state feedback for attitude stabilization of quadrotor," *Int. J. Adv. Robot. Syst.*, vol. 13, no. 1, pp. 2-2, 2016. https://doi.org/10.5772/61934.

[19] S. K. Hong and Y. Nam, "Stable fuzzy control system design with pole-placement constraint: An LMI approach," *Comput. Ind.*, vol. 51, no. 1, pp. 1-11, 2003. https://doi.org/10.1016/S0166-3615(03)00057-5.